
Sequential Likelihood-Free Inference with Implicit Surrogate Proposal

Dongjun Kim

Kyungwoo Song

YoonYeong Kim

Yongjin Shin

Il-Chul Moon

KAIST, Republic of Korea

{dongjoun57,gtshs2,yoonyeong.kim,yj.shin,icmoon}@kaist.ac.kr

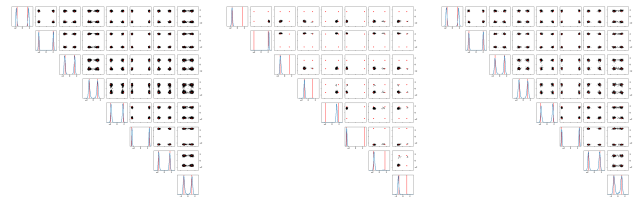
Abstract

Bayesian inference without the access of likelihood, called *likelihood-free inference*, is highlighted in *simulation* to yield a more realistic simulation result. Recent research updates an approximate posterior sequentially with the cumulative simulation input-output pairs over inference rounds. This paper observes that previous algorithms with Monte-Carlo Markov Chain present low accuracy for inference on a simulation with a multi-modal posterior due to the mode collapse of MCMC. From the observation, we propose an implicit sampling method, Implicit Surrogate Proposal (ISP), to draw balanced simulation inputs at each round. The resolution of mode collapse comes from two mechanisms: 1) a flexible surrogate proposal density estimator and 2) a parallel explored samples to train the surrogate density model. We demonstrate that ISP outperforms the baseline algorithms in multi-modal simulations.

1 Introduction

Many disciplines of science, engineering, and economics rely on simulation models. A simulation imitates the real-world with a synthetically designed data-generation process, and this requires a number of interpretable input parameters to a simulation. When we build a simulation model, we ultimately end up with a set of non-calibrated unobservable simulation inputs, which lead to different underlying dynamics that may deviate from the real-world.

Constructing a realistic simulation, by optimizing un-



(a) samples from true posterior (b) Samples from slice sampler (c) Samples from ISP

Figure 1: On SLCP-256 simulation (see Appendix A) with a 256-modal posterior, samples from ISP visits every mode (red points) and share identical structures with samples from true posterior

observable simulation input parameters, has been an important task in the simulation studies. However, the likelihood, $p(x|\theta)$, is unavailable because a simulation is described as a generative process, not an explicit generative distribution, where x is an output and θ is an input. Therefore, *likelihood-free inference* is well applicable to this context as a form of Bayesian inference without access to the likelihood evaluation.

Likelihood-free inference is particularly challenging if the posterior distribution of a simulation is multi-modal (Franck and Koutsourelakis, 2017; Lu et al., 2017). A multi-modality on posterior may arise if any of the three conditions satisfy. First, if the input space is too large, then the posterior would be multi-modal. This happens when we optimize simulations with a few knowledge on the simulation behavior in terms of the inputs. Second, if the sparse real-world observation is given in an aggregated form, there could be multiple inputs that yield the identical aggregated dynamics, even if the underlying component-wise dynamics are distinguished by different parameter sets. Lastly, if the summary statistics is not sufficient, then the statistics of different underlying dynamics could be the same, and the posterior becomes multi-modal.

Recent research on *likelihood-free inference* sequentially approximates the posterior with a cumulative simulation input-output dataset across the inference

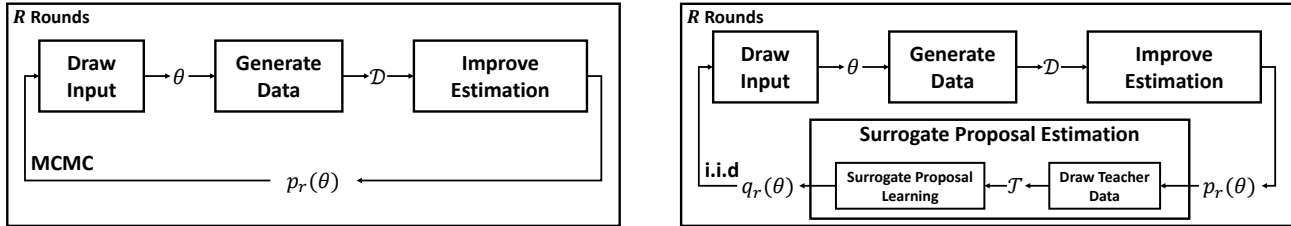


Figure 2: Component view of SLFI with MCMC (Left) and SLFI with ISP $q_r(\theta)$ (Right)

rounds. The sequential algorithm gathers additional N data instances at every round by running additional N simulations with N inputs provided from the algorithm. Afterward, the algorithm estimates the posterior, $p(\theta|x_o)$, from the cumulated dataset over the rounds, where x_o is the real-world observation.

The branches of sequential algorithm approximate the posterior distribution by estimating either 1) the likelihood in Sequential Neural Likelihood (SNL) (Papamakarios and Murray, 2016) and 2) the likelihood-to-evidence ratio in Amortized Approximate Likelihood Ratio (AALR) (Hermans et al., 2020). SNL and the sequential AALR¹ do not have access to the numerical evaluation of the approximate posterior (see Appendix B). Instead, they only allow drawing simulation inputs from the approximate posterior by Monte-Carlo Markov Chain (MCMC). On the other hand, another branch, Automatic Posterior Transformation (APT) (Greenberg et al., 2019), estimates the posterior directly.

The likelihood-based algorithms, SNL and AALR, take advantage of APT that they 1) enable hypothesis tests (Brehmer et al., 2018) and 2) allow prior to change during inference while APT does not allow that (Cranmer et al., 2020). Besides, SNL and AALR provide better performance than APT on simulations with simple likelihoods.

The problem of SNL and AALR originates from MCMC on simulations with complex posteriors. MCMC is known to draw samples from a few modes, leading to SNL and AALR to infer the posterior distribution with only partial modes. This mode collapse becomes more severe as 1) the simulation attains a highly multi-modal posterior, and 2) the simulation output becomes high dimensional.

This paper suggests a new sampling algorithm of *likelihood-free inference*, Implicit Surrogate Proposal (ISP), to resolve the problems of MCMC when we draw simulation inputs. This is the first work of implicit sampler that enhances the sample efficiency in

¹AALR without sequential rounds has access to the numerical evaluation of posterior, but it requires extremely many data instances to learn.

likelihood-based sequential algorithms on *likelihood-free inference* that utilizes MCMC on input sampling. Specifically, ISP improves the sample efficiency by drawing i.i.d simulation inputs from an implicit surrogate proposal distribution. In consequence, ISP reduces the required simulation budget to achieve the desired inference performance compared to the previous works, by improving the approximate posterior with more diverse data instances. The experiments show that SNL with ISP and AALR with ISP are robust on simulations with multi-modal posteriors.

2 Preliminary

2.1 Problem Formulation

A simulation is *likelihood-free*, i.e., no information on the likelihood², $p(x|\theta)$, is accessible because the simulation only allows generating data by *forward* computations. This paper assumes that we have 1) a given prior distribution, $p(\theta)$, and 2) a single-shot real-world observation, x_o . The objective of *likelihood-free inference* is estimating the posterior distribution, $p(\theta|x_o)$, with a limited simulation budget and without access to the exact likelihood of $p(x|\theta)$.

2.2 Sequential Likelihood-Free Inference

Sequential Likelihood-Free Inference (SLFI) iteratively estimates the approximate posterior distribution, $q_r^\phi(\theta|x_o)$, parametrized by ϕ , at each round, r . These recurrent rounds fasten the approximate posterior to the true posterior, $q_r^\phi(\theta|x_o) \rightarrow p(\theta|x_o)$. The algorithm iterates the following steps at each round:

1. **Draw Input** Draw simulation inputs, $\{\theta_{r,j}\}_{j=1}^N$, from the proposal distribution, $p_r(\theta)$.
2. **Generate Data** Add the simulation input-output pairs to the dataset, $\mathcal{D} = \mathcal{D} \cup \{\theta_{r,j}, x_{r,j}\}_{j=1}^N$, by executing the simulation N -times with simulation inputs, $\{\theta_{r,j}\}_{j=1}^N$.

²which is indeed conditional likelihood having θ as context.

3. Improve Estimation

Estimate the approximate density by optimizing a loss $\mathcal{L}(\phi)$ with dataset \mathcal{D} .

The recent algorithms of SLFI share the above algorithm structure, as in Figure 2 (a), with variations on the details of **Improve Estimation** and **Draw Input**. In **Improve Estimation**, there are three branches of likelihood-free inference: likelihood estimation (SNL), ratio estimation (AALR), and posterior estimation (APT). In **Draw Input**, an approach draws i.i.d samples directly in case of estimating a normalized density (APT), and the other approach searches the sample space via MCMC in case of estimating an unnormalized density (SNL and AALR). The following subsections introduce SNL and AALR, and APT will be explained in Section 6.

2.3 Sequential Neural Likelihood

SNL (Papamakarios and Murray, 2016; Lueckmann et al., 2019) estimates the approximate likelihood, $p(x|\theta)$, at **Improve Estimation**. SNL maximizes the log conditional likelihood

$$\mathcal{L}_{SNL}(\phi) = \mathbb{E}_{\tilde{p}(\theta, x)}[\log q^\phi(x|\theta)], \quad (1)$$

which is equivalent to minimize the KL divergence, $D_{KL}(\tilde{p}(\theta)p(x|\theta) \parallel \tilde{p}(\theta)q^\phi(x|\theta))$. Hence, the optimal likelihood, $q^*(x|\theta)$, estimates the exact likelihood, $p(x|\theta)$, on the support of $\tilde{p}(\theta) = \frac{1}{r} \sum_{r'=1}^r p_{r'}(\theta)$.

In each round, the inference algorithm draws N simulation inputs, $\{\theta_{r,j}\}_{j=1}^N$, from the proposal distribution, $p_r(\theta)$. SNL designs this proposal distribution to be proportional to $q_r^\phi(x_o|\theta)p(\theta)$. Here, the proposal distribution becomes an approximate posterior on θ , where $p(\theta)$ is the base prior distribution. As the approximate posterior converges to the true posterior, the proposal distribution is more likely to sample the next θ near the peak of the true posterior. This proposal setting improves sample quality as the round proceeds, and eventually, the likelihood, $p(x_o|\theta)$, around $x = x_o$ is tightened.

Original SNL uses the slice sampler to draw samples. However, as depicted in Figure 1 (b), MCMC does not visit every mode within the simulation budget due to the slow-mixing, and this motivates developing a surrogate feed-forward sampler instead of MCMC in drawing simulation inputs. We introduce a surrogate sampler in Section 3, and we investigate the advantages of ISP over MCMC in Section 4.

2.4 Amortized Approximate Likelihood Ratio

Hermans et al. (2020) introduced AALR to estimate the likelihood-to-evidence ratio, $r(x|\theta) = p(x|\theta)/p(x)$,

at **Improve Estimation**. The estimation originates from the classification of the input-output pairs, (θ, x) , from 1) the joint distribution, $\tilde{p}(\theta, x)$, with a class label, $y = 1$; and from 2) the mean-field distribution, $\tilde{p}(\theta)\tilde{p}(x)$, with a class label, $y = 0$, where $\tilde{p}(x) = \int p(x|\theta)\tilde{p}(\theta)d\theta$. Therefore, AALR maximizes the binary cross entropy loss as Eq. 2.

$$\begin{aligned} \mathcal{L}_{AALR}(\phi) &= \mathbb{E}_{\tilde{p}(\theta, x)}[\log d^\phi(\theta, x)] \\ &+ \mathbb{E}_{\tilde{p}(\theta)\tilde{p}(x)}[\log(1 - d^\phi(\theta, x))]. \end{aligned} \quad (2)$$

The optimal classifier (or discriminator) of the binary cross entropy loss becomes

$$d^*(\theta, x) = \frac{\tilde{p}(\theta, x)}{\tilde{p}(\theta, x) + \tilde{p}(\theta)\tilde{p}(x)},$$

which is equivalent to

$$\frac{d^*(\theta, x)}{1 - d^*(\theta, x)} = \frac{\tilde{p}(\theta, x)}{\tilde{p}(\theta)\tilde{p}(x)} = \frac{p(x|\theta)}{\tilde{p}(x)}.$$

Therefore, AALR estimates the likelihood-to-evidence ratio by $r^\phi(x|\theta) := \frac{d^\phi(\theta, x)}{1 - d^\phi(\theta, x)}$.

One could adopt the sequential approach to the above AALR in order to scale down the required simulation budget for the inference. At the sampling procedure, the new inputs, $\{\theta_{r,j}\}_{j=1}^N$, to be simulated are drawn from the proposal distribution, $p_r(\theta)$, which is proportional to $r_r^\phi(x_o|\theta)p(\theta)$. Analogous to SNL, the original AALR makes use of MCMC, because the proposal distribution in AALR is unnormalized in terms of θ , i.e., $p_r(\theta) \propto r_r^\phi(x_o|\theta)p(\theta)$.

3 Methodology

This section introduces the suggested sampling algorithm, or Implicit Surrogate Proposal (ISP). First, we explain the details of ISP, and we discuss its properties in Section 4.

3.1 Sequential Likelihood-Free Inference with Implicit Surrogate Proposal

The suggested sampler of ISP draws samples from an implicit surrogate proposal distribution, $q_r^\psi(\theta)$, of the original proposal distribution, $p_r(\theta)$. Here, the original proposal distribution is 1) $p_r(\theta) \propto q_r^\phi(x_o|\theta)p(\theta)$ in SNL and 2) $p_r(\theta) \propto r_r^\phi(x_o|\theta)p(\theta)$ in AALR. After approximating $p_r(\theta)$ with $q_r^\psi(\theta)$, ISP generates feed-forward samples, $\{\theta_{r,j}\}_{j=1}^N$, in a fully independent way, so the surrogate sampler alleviates the problems of MCMC.

Figure 2 (b) illustrates the suggested algorithm in a component view. The suggested algorithm adds an

auxiliary structure, **Surrogate Proposal Estimation**, upon the three basic steps of the sequential algorithm structure introduced in Section 2.2. The **Surrogate Proposal Estimation** step includes two sub-steps, **Draw Teacher Data** and **Surrogate Proposal Learning**, in order to train an implicit proposal distribution. **Draw Teacher Data** collects the training data from the original proposal distribution, and **Surrogate Proposal Learning** estimates a surrogate proposal distribution with the gathered teacher dataset. After estimating a surrogate proposal, the sequential algorithm draws a batch of simulation inputs, $\{\theta_{r,j}\}_{j=1}^N$, in the **Draw Input** step from the estimated surrogate proposal distribution, $q_r^\psi(\theta)$, instead of the original proposal distribution, $p_r(\theta)$. Afterward, the step of **Generate Data** supplies the corresponding simulation result, $\{x_{r,j}\}_{j=1}^N$, and **Improve Estimation** updates the conditional density from either 1) Eq. 1 in SNL and 2) Eq. 2 in AALR. Putting all together, the process of the sequential likelihood-free inference with ISP is as below.

1. **Draw Input** Draw simulation inputs, $\{\theta_{r,j}\}_{j=1}^N$, from the surrogate proposal distribution, $q_r^\psi(\theta)$.
2. **Generate Data** Same with Section 2.2.
3. **Improve Estimation** Same with Section 2.2.
4. **Surrogate Proposal Estimation**
 - (a) **Draw Teacher Data** Draw the training data, \mathcal{T} , from the proposal distribution, $p_r(\theta)$, by the Metropolis-Hastings sampler with multi-chains.
 - (b) **Surrogate Proposal Learning** Estimate the surrogate proposal distribution, $q_r^\psi(\theta)$, by optimizing a loss $\mathcal{L}(\psi)$ in Eq. 3 with the collected teacher dataset, \mathcal{T} .

Algorithm 1 presents the detailed processes of the sequential likelihood-free inference with ISP.

The following subsections provide the details of the inference steps. We start from **Draw Teacher Data** to highlight the learning of the implicit surrogate proposal distribution.

3.2 Draw Teacher Data

Draw Teacher Data extracts the training dataset from the original proposal distribution, $p_r(\theta)$, estimated in the **Improve Estimation** step. From the M number of Markov chains, we collect M data instances, $\mathcal{T} = \{\theta_{B+1}^m\}_{m=1}^M$, where each θ_{B+1}^m is drawn from a single chain of the Metropolis-Hastings (M-H) sampler independently (Crăiu et al., 2009; Llorente et al.,

Algorithm 1: Sequential Likelihood-Free Inference with Implicit Surrogate Proposal

```

1 for  $r = 1$  to  $R$  do
2   Draw a batch of samples  $\{\theta_{r,j}\}_{j=1}^N \sim q_r^\psi(\theta)$ 
   from the surrogate proposal
3   for  $j = 1$  to  $N$  do
4     Simulate  $x_{r,j} \sim p(x|\theta_{r,j})$ 
5   Add  $(\theta_{r,j}, x_{r,j})$  into the training data
    $\mathcal{D} \leftarrow \mathcal{D} \cup \{(\theta_{r,j}, x_{r,j})\}_{j=1}^N$ 
6   while not converged do
7     Update  $\phi$  to maximize  $\mathcal{L}(\phi)$  (Eq. 1 or Eq.
   2) with data  $\mathcal{D}$ 
8   Generate teacher data  $\mathcal{T}$  from the proposal
    $p_r(\theta)$  by MCMC with multi-chains
9   Re-initialize posterior parameter  $\psi$ 
10  while not converged do
11    Update  $\psi$  to maximize  $\mathcal{L}(\psi)$  (Eq. 3) with
   data  $\mathcal{T}$ 

```

2019) after the burn-in period, B . For an individual Markov chain, the M-H sampler's m -th chain draws an intermediate state, $(\theta_{b+1}^m)'$, from the proposal distribution, $q^m(\theta'|\theta_b^m) = \mathcal{N}(\theta_b^m, \sigma^2 I)$, and M-H accepts $(\theta_{b+1}^m)'$ with the acceptance probability. Below is the acceptance probability of SNL of the m -th chain.

$$\alpha^m(\theta'|\theta_b^m) = \min \left(\frac{q^m(\theta_b^m|\theta')p(\theta')q_r^\phi(x_o|\theta')}{q^m(\theta'|\theta_b^m)p(\theta_b^m)q_r^\phi(x_o|\theta_b^m)}, 1 \right).$$

Below is the acceptance probability of AALR.

$$\alpha^m(\theta'|\theta_b^m) = \min \left(\frac{q^m(\theta_b^m|\theta')p(\theta')r_r^\phi(x_o|\theta')}{q^m(\theta'|\theta_b^m)p(\theta_b^m)r_r^\phi(x_o|\theta_b^m)}, 1 \right),$$

We adaptively choose the variance of the proposal distribution, $q^m(\theta'|\theta)$, for each chain independently, according to (Roberts et al., 1997). As M increases, the samples from M-H with M chains are distributed by the proposal distribution.

3.3 Surrogate Proposal Learning

The loss of the surrogate proposal is the log likelihood, parametrized by ψ , as

$$\mathcal{L}(\psi) = \mathbb{E}_{p_r(\theta)} [\log q_r^\psi(\theta)]. \quad (3)$$

The maximization of the loss is equivalent to the minimization of the KL divergence, $D_{KL}(p_r(\theta)||q_r^\psi(\theta))$. The KL divergence is minimized if the surrogate estimates the exact proposal, so the loss function enforces the optimal surrogate proposal to approximate the exact proposal distribution as $q_r^*(\theta) = p_r(\theta)$.

This paper suggests using a normalizing flow as the surrogate model of the proposal distribution, $q_r^\psi(\theta)$, to satisfy a pair of functionalities. First, a flow model enables to draw samples via feed-forward computations,

$$\{\theta_{r,j}\}_{j=1}^N = \{\mathbf{f}_r^\psi(z_j)|z_j \sim \mathcal{N}(0, I) \text{ for } j = 1, \dots, N\},$$

where $\mathbf{f}_r^\psi = (f^{(1)}, \dots, f^{(K)})$ is the estimated transformations of a flow model in the **Surrogate Proposal Learning** step. These feed-forward samples entirely depend on the random noises, z_j , from the standard Gaussian distribution. Therefore, if the surrogate proposal estimates the original proposal distribution accurately, ISP provides a set of i.i.d samples for the next simulation inputs from the original unnormalized proposal distribution.

Second, the surrogate proposal, $q_r^\psi(\theta)$, enables evaluating the posterior numerically. The target distribution of a surrogate proposal will approximate the original proposal distribution, which is designed to be the approximate posterior: $p_r(\theta) = q_r^\phi(\theta|x_o)$. Originally, SNL and the sequential AALR does not allow to evaluate the density for the approximate posterior, since the Bayes rule only provides an unnormalized proposal distribution. This functionality provides access to the approximate posterior density to SNL and the sequential AALR.

3.4 Normalizing Flow for Surrogate Proposal

A recent study on the normalizing flow develops Neural Spline Flow (NSF) (Durkan et al., 2019), allowing both the density estimation and the sampling in a single pass. According to (Durkan et al., 2019), NSF is a flexible flow model that could capture multiple modes. NSF transforms $\mathcal{N}(0, I)$ into $q^\psi(\theta)$ through the coupling transformations, $\mathbf{f}^\psi = (f^{(1)}, \dots, f^{(K)})$. NSF generates a sample, $\theta \sim q^\psi(\theta)$, by the forward transformation:

$$\theta = z^{(K)} \quad \text{where} \quad z^{(0)} \sim \mathcal{N}(0, I), z^{(k)} = f^{(k)}(z^{(k-1)}).$$

The density of θ generated from the flow is obtained by the following change of variable:

$$q^\psi(\theta) = \mathcal{N}((f^{(1)})^{-1} \circ \dots \circ (f^{(K)})^{-1}(\theta); 0, I) \times \prod_{k=1}^K \left| \det \left(\frac{\partial f^{(k)}}{\partial z^{(k-1)}} \right) \right|^{-1}.$$

NSF models each coupling transformation, $f^{(k)}$, with a number of rational spline functions, where each function is a monotonic rational-quadratic spline.

4 Discussion

SNL and AALR draw simulation inputs from MCMC, as described in Figure 2 (a). There are three prac-

Table 1: Comparison of the multi-chain MCMC and the surrogate proposal

DIAGNOSTIC	SLICE SAMPLER		METROPOLIS-HASTINGS SAMPLER				IMPLICIT SURROGATE PROPOSAL
	# CHAINS		# CHAINS				
	1	10	1	10	100	1,000	
<i>Missed Mode</i>	247 (±2.4)	195 (±9.47)	248 (±2.24)	229 (±2.96)	157 (±4.27)	14 (±2.95)	7 (±2.34)
<i>Sample Imbalance</i>	1.93 (±0.02)	1.55 (±0.06)	1.93 (±0.03)	1.79 (±0.02)	1.30 (±0.03)	0.55 (±0.03)	0.44 (±0.02)
<i>Sampling Time*</i>	3006 (±86)	1055 (±17)	85.79 (±0.21)	8.76 (±0.07)	1.03 (±0.11)	0.26 (±0.00)	0.02 (±0.00)

* WE USED INTEL XEON E5-2560 V3 CPU AND NVIDIA TITAN XP GPU. THE UNIT IS SECOND.

tical problems of MCMC in likelihood-free inference. The first is the *mode collapse* problem because of slow-mixing, the second is the *sample imbalance* problem, and the last is the slow *sampling time* problem.

To empirically analyze the three problems, we draw 1,000 samples from the approximate posterior estimated by SNL with ISP after ten rounds of inference on SLCP-256 simulation (see Appendix A), where SLCP-256 attains 256 modes in its posterior. Figure 1 and Table 1 are the results of the experiment. The samples are drawn by 1) the slice sampler with a single chain and 10 number of chains, 2) the M-H sampler with 1, 10, 100, and 1,000 chains, and 3) the implicit surrogate proposal. MCMC with L -chains draws $1,000/L$ number of samples from each chain. We apply the thinning method (Owen, 2017) to avoid each chain’s auto-correlation: each MCMC chain discards all but every ten samples after the 20 burn-in period. No more than 1,000 chains are available because there is a total of 1,000 samples.

4.1 Mode Collapse

When the simulation output is high dimensional, the likelihood, $p(x_o|\theta)$, is more localized to a small region in θ -space, so the area of non-zero likelihood in θ -space becomes sparse. In such a case, MCMC is more likely to fail at exploring the search space after falling into a local mode (Betancourt, 2017) because a sample cannot jump from a local optimum to another optimum by passing through a region with almost zero-probability (Andrieu and Thoms, 2008).

Suppose MCMC fails at exploring near a mode, $\hat{\theta}$. In that case, the estimation is not tightened up near $\hat{\theta}$ because there are a few training instances at \mathcal{D} to elaborate the approximate posterior near $\hat{\theta}$. In other words, the sample quality and the estimation accuracy reinforce each other: the low sample quality will result in the poor estimation around a particular area of θ -space. In reverse, poor estimation may skip exploring the poorly sampled area in future. Therefore, the improvement in the inference hinges upon the sampling technique of informative instance in \mathcal{D} .

Figure 1 (b) presents that the slice sampler with a single chain fails at capturing multi-modals in the ground-truth posterior distribution presented in Figure 1 (a). *Missed Mode* counts the number of modes that have no neighboring samples³ out of 1,000 samples. Table 1 presents the consistent performance with Figure 1 in the slice sampler with a single chain. In addition, the quantitative result shows that the M-H sampler differs on a minor scale from the slice sampler if only a single chain is applied.

On the other hand, the multi-chain MCMC dramatically reduces *Missed Mode*. Table 1 presents that the slice sampler with ten chains misses 195 modes out of a total of 256 modes. In particular, M-H with 1,000 chains only misses 14 modes out of 256. This 14 gives the lower bound of M-H with multi-chains.

On top of that, ISP captures all but seven modes out of 256 modes. *Missed Mode* in ISP is halved over the lower bound of M-H with multi-chains because a flexible estimator learns ISP with the teacher training dataset, which attains 5,000 training instances drawn from M-H with 5,000 chains.

4.2 Sample Imbalance

Besides of the mode collapse, MCMC may lead sample imbalance if the samples are auto-correlated. *Sample Imbalance* quantitatively measures how the 1,000 samples are imbalanced. *Sample Imbalance* measures the L^1 norm of a 256-dimensional vector, which is the deviation between the sample distribution on modes and the uniform distribution. The ideal samples are distributed uniformly for every mode, so the lower *Sample Imbalance* represents more balanced samples.

Table 1 presents that the *Sample Imbalance* of the slice sampler and the M-H sampler with a single chain are identical. However, the M-H sampler with 1,000 chains drops the performance to 0.55 from 1.93. The implicit surrogate proposal improves the performance from the lower bound (0.55) of the multi-chain MCMC to 0.44. The improved *Sample Imbalance* guarantees the reduced number of required simulation budget to achieve the desired performance.

4.3 Sampling Time

The sampling time becomes problematic if we use a flexible conditional density model in the **Improve Estimation** step to capture the multi-modal posterior. The complex model eventually leads **Draw Sample** to be a bottleneck of the inference if MCMC sampling time is slow, since every step in MCMC requires a

³We consider a sample as a neighbor of a mode if two points are in the same orthant.

Table 2: Complexity analysis

ALGORITHM	DRAW INPUT	IMPROVE ESTIMATION	DRAW TEACHER DATA	SURROGATE PROPOSAL LEARNING
APT	$O(RNF_c)$	$O(R^2NE_cB_c)$	—	—
SNL/AALR	$O(RNTLF_c)$	$O(R^2NE_cB_c)$	—	—
SNL WITH ISP/AALR WITH ISP	$O(RNF_s)$	$O(R^2NE_cB_c)$	$O(RMTLF_c)$	$O(RME_sB_s)$

number of expensive model evaluations.

Table 1 presents *Sampling Time* by the slice sampler and the M-H sampler. The slice sampler with a single chain takes nearly an hour (3006 seconds) to draw 1,000 samples from the approximate posterior. The slice sampler with ten chains takes nearly one-third over the slice sampler with a single chain. In comparison, M-H with ten chains is ten times faster than M-H with a single chain because the M-H sampler’s algorithm design enables us to update all the chains simultaneously with batch computations. This batch update of M-H chains dramatically reduces the sampling time from 86 seconds to 0.26 seconds. Moreover, ISP takes only 0.02 seconds to draw 1,000 samples. The fast sampling time of ISP comes from the feed-forward computations without any of burn-in period.

5 Complexity Analysis

Table 2 compares the computational burdens in the big-O notation of SLFI with/without ISP. Other than the simulation run time, four building blocks take the computational burden: 1) **Draw Input**, 2) **Improve Estimation**, 3) **Draw Teacher Data**, 4) **Surrogate Proposal Learning**.

In order to analyze the complexity, we give the following assumptions. First, we assume that the forward and the backward computations of the conditional density require F_c and B_c operations, respectively. Here, the magnitudes of F_c and B_c fully depend on a flow estimator for conditional density. Analogously, we denote F_s and B_s as the forward/backward computations of the surrogate proposal density.

Second, although we use the early stopping in our experiments, in order to analyze, we assume E_c epochs and E_s epochs to train the conditional density and the surrogate density, respectively. Third, we assume that MCMC evaluates the conditional density L times per state transition on average, even though every state requires a different number of conditional density evaluations to update a state. Fourth, the complexities are measured for the total computations across R rounds.

Table 2 presents that the complexities of all but **Im-**

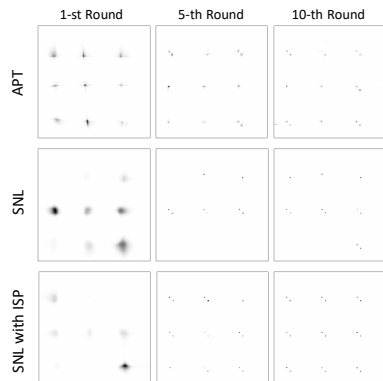


Figure 3: Approximate posteriors on Shubert simulation as the round proceeds

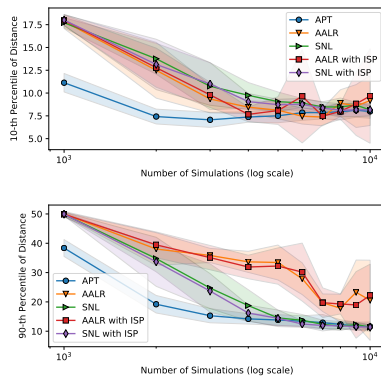


Figure 4: Top 10-th percentile (above) and 90-th (below) of distance on SLCP-16 simulation

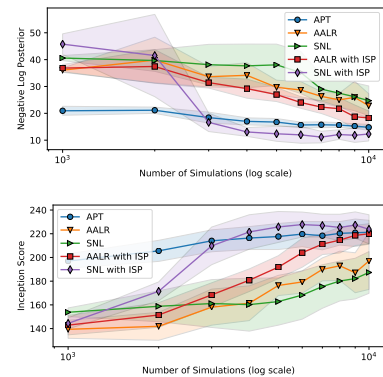


Figure 5: Negative log posterior and inception score on SLCP-256 simulation

prove Estimation increases linearly with R . The complexity of **Improve Estimation** increases as R -square because the cumulative simulation dataset up to the r -th round, $\mathcal{D} = \{(\theta_{r',j}, x_{r',j}) | r' = 1, \dots, r, j = 1, \dots, N\}$, has rN number of training instances. Therefore, the total complexity is dominated by the **Improve Estimation** step, if 1) F_c, B_c, F_s and B_s , 2) E_c and E_s , and 3) N and M are valued on the same scale, and 4) T and L are not significantly large.

6 Related Work

Approximate Bayesian Computation (ABC) (Tavaré et al., 1997) estimates the posterior with accepted inputs that have the simulation outcome within ϵ -ball of the real-world observation. SMC-ABC (Sisson et al., 2007) utilizes the sequential Monte-Carlo in searching the input space, and the posterior becomes a smoothed, weighted empirical distribution, where the kernel evaluation obtains the weights.

There are sequential approaches that do not rely on MCMC in **Draw Sample**. Sequential Neural Posterior Estimation (SNPE) estimates the posterior distribution at **Improve Estimation** to draw feed-forward samples from the estimated posterior. APT/SNPE-C (Greenberg et al., 2019) suggests a loss, $\mathcal{L}_{APT}(\phi) = \mathbb{E}_{\tilde{p}(x,\theta)} \left[\log q^\phi(\theta|x) \frac{\tilde{p}(\theta)}{p(\theta)} \frac{1}{\int q^\phi(\theta|x) \frac{\tilde{p}(\theta)}{p(\theta)} d\theta} \right]$, to obtain an approximate posterior. Maximizing the loss function is equivalent to minimizing the KL divergence, $D_{KL}(p(x)p(\theta|x) || p(x)q^\phi(\theta|x))$, so APT's optimal density matches the exact posterior distribution. To make the integration of $\int q^\phi(\theta|x) \frac{\tilde{p}(\theta)}{p(\theta)} d\theta$ tractable, the hypothesis class of the proposal distribution in APT is limited to a simple densities form.

7 Experiments

We compare SNL with ISP and AALR with ISP over SNL, AALR, APT, and SMC-ABC. We use NSF for both the surrogate proposal distribution and the conditional distribution, except for AALR and ISP-based AALR. We use MLPs for the conditional estimator in AALRs. See Appendix C for the detailed setup.

7.1 Simulation Setting

This paper experiments the ISP on tractable simulations with multi-modal posteriors. First, the Shubert simulation, based on the Shubert function (Jamil and Yang, 2013), has 18 modes in its posterior, and the simulation budget is $N = 5,000$ for each round. The other remaining tractable simulations generalize the benchmark SLCP (Papamakarios and Murray, 2016; Greenberg et al., 2019). SLCP-16 has five-dimensional inputs, 50-dimensional outputs, and a 16-modal posterior. SLCP-256 has eight-dimensional inputs, 40-dimensional outputs, and 256 modes in posterior. Two SLCP models share the simulation budget as $N = 1,000$ for each round.

This paper also experiments with two simulations that describe the real-world: M/G/1 (Shestopaloff and Neal, 2014) and Competitive Lotka Volterra (CLV) (Vano et al., 2006). CLV is a generalization of the benchmark Lotka Volterra simulation in order to yield a posterior with two modals. CLV has eight-dimensional inputs and ten-dimensional outputs. We describe the details of the simulations in Appendix A.

7.2 Results

Figure 3 presents the approximate posteriors over the rounds on the Shubert simulation. APT shows a better

Table 3: Performance of tractable simulation models

ALGORITHM	SAMPLING	# CHAINS	SHUBERT			SLCP-16			SLCP-256		
			$-\log p(\theta x_o)$	log MMD	IS	$-\log p(\theta x_o)$	log MMD	IS	$-\log p(\theta x_o)^*$	log MMD	IS
SMC-ABC	EMPIRICAL	—	98.58±1.82	-1.16±0.01	9.54±0.40	139.02±4.21	-2.56±1.68	8.87±0.39	38.80±0.41	-6.36±0.15	222.49±3.07
APT	DIRECT	—	38.54±11.76	-1.12±0.08	14.24±0.98	5.97±12.05	-1.83±0.85	13.27±2.04	14.78±1.09	-6.02±0.64	221.25±10.06
SNL	SLICE	1	31.64±16.10	-0.62±0.21	13.96±1.17	10.24±7.09	-1.09±0.03	13.88±0.95	24.70±5.50	-1.52±0.32	187.34±17.56
		10	16.14±6.64	-1.28±0.81	14.87±0.86	8.62±4.86	-1.76±0.67	13.64±1.18	14.43±3.06	-1.36±0.23	222.60±9.28
	M-H	1	43.01±41.88	-0.53±0.14	14.21±0.84	-11.04±25.34	-0.99±0.03	15.76±0.33	23.94±8.63	-1.01±0.05	209.47±15.58
		100	44.42±66.46	-4.83±0.80	15.32±0.96	-18.01±13.47	-5.71±0.69	15.72±0.47	17.38±8.51	-5.62±0.47	217.44±12.81
AALR	SLICE	1	57.88±4.74	-3.34±1.45	11.85±0.60	65.09±9.44	-1.48±0.74	10.97±0.61	21.25±4.07	-3.37±0.03	209.50±10.61
		10	62.99±8.31	-3.04±0.82	11.51±0.45	49.17±12.52	-2.79±0.43	12.02±0.76	16.56±1.28	-3.47±0.07	215.75±12.90
	M-H	1	63.35±8.15	-3.47±0.90	10.98±0.98	50.01±20.49	-1.11±0.15	12.55±1.18	22.82±4.49	-1.01±0.05	197.03±23.96
		100	59.60±3.12	-4.44±0.79	11.12±0.63	42.42±28.07	-3.83±0.67	14.03±0.91	19.97±2.18	-5.62±0.47	215.78±9.69
SNL	ISP	—	2.18±23.43	-5.56±0.79	15.64±0.74	-32.11±19.70	-7.02±0.95	15.85±0.29	12.30±2.58	-6.87±0.64	223.77±12.22
AALR		—	61.56±4.41	-4.86±1.06	11.24±0.62	31.56±19.43	-3.68±0.53	12.95±1.69	18.28±2.54	-5.78±1.18	220.00±8.38

* SCALED BY 10^{-2}

performance in the early stage of inference, but SNL eventually outperforms APT as round proceeds due to the overfitting in APT. The overfitting occurs in APT because APT approximates the posterior by the point estimation at $x = x_o$. On the other hand, SNL avoids this overfitting issue because SNL estimates the posterior by Bayesian inference. Consequently, the shape of each mode in SNL looks more spherical compare to APT, where the ground-truth shape of each mode is a sphere. On top of that, SNL with ISP captures every mode in Figure 3 by constructing more diverse training data for likelihood estimation.

Figure 4 shows the simulation L^2 discrepancy to the observation on SLCP-16. Analogous to the Shubert simulation, APT on SLCP-16 performs the best in the first round, but SNL approaches catch up the performance at the end of inference. Also, Figure 4 shows indistinguishable performance between SNL with/without ISP because the simulation L^2 distance degrades after the inference captures at least a single mode. The 10-th percentile and the 90-th percentile distances perform similarly for APT and SNL at the end. This implies that the simulation L^2 distance of APT and SNL are distributed similarly after rounds.

Figure 5 shows the negative log posterior, $-\sum_{i=1}^{256} \log p(\theta_i^*|x_o)$, at ground-truth modes, and the Inception Score (IS) (Salimans et al., 2016) of SLCP-256, where IS measures the sample diversity (see Appendix D). SNL with ISP consistently outperforms SNL in Figure 5 for both performances. In particular, the introduction of ISP in SNL provides a statistically significant performance gain against APT, where SNL is unable to compete with APT. In addition, the performances of AALR with ISP are increased over AALR.

Table 3 demonstrates that SNL with ISP outperforms in every performance metric on every tractable simulation. This indicates three empirical results: 1) SNL

Table 4: Performance of real-world simulation models

ALGORITHM	SAMPLING	# CHAINS	M/G/1	CLV
			$-\log p(\theta x_o)$	$-\log p(\theta x_o)$
SMC-ABC	EMPIRICAL	—	3.89±1.10	16.77±4.60
APT	DIRECT	—	-0.48±0.95	10.05±1.60
SNL	SLICE	1	-0.99±0.29	10.06±1.98
		10	-0.85±0.41	10.47±2.57
	M-H	1	-0.92±0.58	15.74±6.17
		100	-1.01±0.32	16.54±7.04
AALR	SLICE	1	-0.62±0.26	10.79±1.31
		10	-0.38±0.30	9.95±1.25
	M-H	1	-0.64±0.36	10.79±1.31
		100	-0.57±0.68	10.15±1.44
SNL	ISP	—	-1.12±0.50	13.49±4.11
AALR		—	-0.60±0.43	11.83±1.79

with ISP provides the most accurate inference with the highest posterior at $x = x_o$; 2) the samples from SNL with ISP are distributed closest to the ground-truth posterior, which is indicated by the lowest MMD score; 3) SNL with ISP provides the most diverse samples from the approximate posterior distribution, deduced from the best inception score.

While we note SNL’s advances with ISP in multi-modal cases, Table 4 shows M/G/1 and CLV performances, where M/G/1 attains a unimodal posterior, and CLV has a bi-modal posterior. In M/G/1, SNL with ISP performs best, and we conjecture that the i.i.d property guarantees the best performance. In CLV, SNL with ISP is outperforming the SNL with the M-H sampler, but AALR with the slice sampler on ten chains shows the best performance.

8 Conclusion

This paper suggests the Implicit Surrogate Proposal that draws i.i.d simulation inputs from the proposal.

ISP’s two mechanisms improve the sample quality: 1) a flexible estimator of the proposal, 2) independent teacher training instances from MCMC with multiple chains. The experiments empirically demonstrate that SNL with ISP performs the best among baselines.

References

- Andrieu, C. and Thoms, J. (2008). A tutorial on adaptive mcmc. *Statistics and computing*, 18(4):343–373.
- Betancourt, M. (2017). A conceptual introduction to hamiltonian monte carlo. *arXiv preprint arXiv:1701.02434*.
- Brehmer, J., Cranmer, K., Louppe, G., and Pavez, J. (2018). A guide to constraining effective field theories with machine learning. *Physical Review D*, 98(5):052004.
- Craiu, R. V., Rosenthal, J., and Yang, C. (2009). Learn from thy neighbor: Parallel-chain and regional adaptive mcmc. *Journal of the American Statistical Association*, 104(488):1454–1466.
- Cranmer, K., Brehmer, J., and Louppe, G. (2020). The frontier of simulation-based inference. *Proceedings of the National Academy of Sciences*.
- Durkan, C., Bekasov, A., Murray, I., and Papamakarios, G. (2019). Neural spline flows. In *Advances in Neural Information Processing Systems*, pages 7511–7522.
- Franck, I. M. and Koutsourelakis, P.-S. (2017). Multimodal, high-dimensional, model-based, bayesian inverse problems with applications in biomechanics. *Journal of Computational Physics*, 329:91–125.
- Greenberg, D., Nonnenmacher, M., and Macke, J. (2019). Automatic posterior transformation for likelihood-free inference. In *International Conference on Machine Learning*, pages 2404–2414.
- Hermans, J., Begy, V., and Louppe, G. (2020). Likelihood-free mcmc with amortized approximate ratio estimators. In *International Conference on Machine Learning*.
- Jamil, M. and Yang, X.-S. (2013). A literature survey of benchmark functions for global optimisation problems. *International Journal of Mathematical Modelling and Numerical Optimisation*, 4(2):150–194.
- Llorente, F., Martino, L., and Delgado, D. (2019). Parallel metropolis–hastings coupler. *IEEE Signal Processing Letters*, 26(6):953–957.
- Lu, D., Ricciuto, D. M., Walker, A. P., Safta, C., and Munger, W. (2017). Bayesian calibration of terrestrial ecosystem models: a study of advanced markov chain monte carlo methods. *Biogeosciences (Online)*, 14(18).
- Lueckmann, J.-M., Bassetto, G., Karaletsos, T., and Macke, J. H. (2019). Likelihood-free inference with emulator networks. In *Symposium on Advances in Approximate Bayesian Inference*, pages 32–53. PMLR.
- Owen, A. B. (2017). Statistically efficient thinning of a markov chain sampler. *Journal of Computational and Graphical Statistics*, 26(3):738–744.
- Papamakarios, G. and Murray, I. (2016). Fast ε -free inference of simulation models with bayesian conditional density estimation. In *Advances in Neural Information Processing Systems*, pages 1028–1036.
- Roberts, G. O., Gelman, A., Gilks, W. R., et al. (1997). Weak convergence and optimal scaling of random walk metropolis algorithms. *The annals of applied probability*, 7(1):110–120.
- Salimans, T., Goodfellow, I., Zaremba, W., Cheung, V., Radford, A., and Chen, X. (2016). Improved techniques for training gans. In *Advances in neural information processing systems*, pages 2234–2242.
- Shestopaloff, A. Y. and Neal, R. M. (2014). On bayesian inference for the m/g/1 queue with efficient mcmc sampling. *arXiv preprint arXiv:1401.5548*.
- Sisson, S. A., Fan, Y., and Tanaka, M. M. (2007). Sequential monte carlo without likelihoods. *Proceedings of the National Academy of Sciences*, 104(6):1760–1765.
- Tavaré, S., Balding, D. J., Griffiths, R. C., and Donnelly, P. (1997). Inferring coalescence times from dna sequence data. *Genetics*, 145(2):505–518.
- Vano, J., Wildenberg, J., Anderson, M., Noel, J., and Sprott, J. (2006). Chaos in low-dimensional lotka–volterra models of competition. *Nonlinearity*, 19(10):2391.